Solar Sail Model Validation from Echo Trajectories

Andrew F. Heaton*
NASA Marshall Space Flight Center
Huntsville, AL 35812

Adam T. Brinckerhoff†
University of Michigan
Ann Arbor, MI 48109

The NASA In-Space Propulsion program has been engaged in a project to increase the technology readiness of solar sails. Recently, these efforts came to fruition in the form of several software tools to model solar sail guidance, navigation and control. Furthermore, solar sails are one of five technologies competing for the New Millennium Program Space Technology 9 flight demonstration mission. The historic Echo 1 and Echo 2 balloons were comprised of aluminized Mylar, which is the near-term material of choice for solar sails. Both spacecraft, but particularly Echo 2, were in low Earth orbits with characteristics similar to the proposed Space Technology 9 orbit. Therefore, the Echo balloons are excellent test cases for solar sail model validation. We present the results of studies of Echo trajectories that validate solar sail models of optics, solar radiation pressure, shape and low-thrust orbital dynamics.

INTRODUCTION

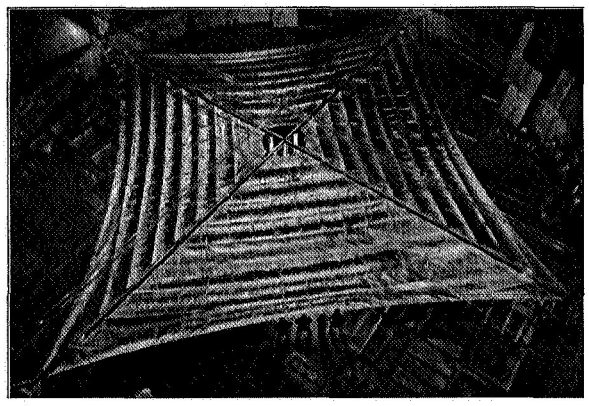

Figure 1 L'Garde 20-meter Solar Sail

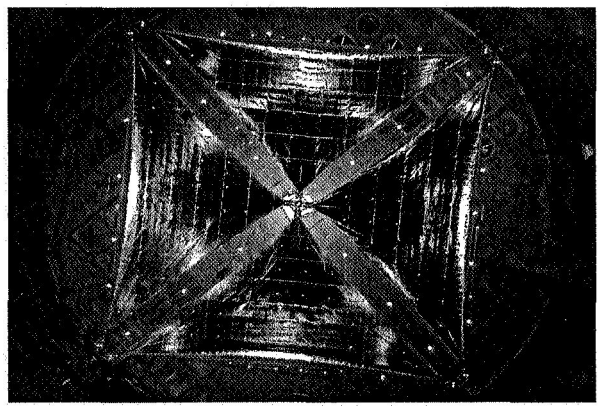

Figure 2 ATK 20-meter Solar Sail

A solar sail is a propulsive device that generates a thrust from reflected solar light pressure. The size of the thrust is a function of the area, mass, and optical properties of the solar sail. NASA's In-Space Propulsion (ISP) recently completed a three-year project[1] to raise the Technology Readiness Level (TRL) of solar sails to a level of 6. A TRL of 6 corresponds to a product that, in summary, is tested on the ground to a point that is just short of a flight

*Senior Engineer, Guidance, Navigation and Control Group, EV42, NASA Marshall Space Flight Center, Huntsville, AL 35812, (256) 544-3839, andrew.f.heaton@nasa.gov, AIAA Member.

†Undergraduate Student, Aerospace Engineering, FXB Building 1320 Beal Avenue Ann Arbor, Michigan 48109, (217) 414-8766, abrinck@umich.edu , AAS Member.

validation. The ISP solar sail project consisted of three "flagship" endeavors. Two of the efforts involved hardware developments that culminated in deployment of two 20-meter square solar sails in a large vacuum chamber in Plumbrook, Ohio (see Figure 1 and Figure 2)[2,3]. The third flagship effort was the creation of a solar sail software package to model all aspects of solar sail Guidance, Navigation, and Control (GN&C) to address control concerns as far as possible in simulation. Control of solar sails is challenging due to the large gossamer structure of the sail, and the low bandwidth of the controllers that may be available.

The ISP GN&C model development effort was headed by the Jet Propulsion Laboratory (JPL). The product, termed the Solar Sail Spaceflight Simulation Software[4] (or S5), consists of five modules. The five modules are designed to model solar radiation pressure, low thrust optimization, thrust control, attitude dynamics/control, and navigation. For the analysis presented in this paper, the solar radiation pressure (or SRP) module and the low thrust optimization (or OPT) module are of primary interest, and for the OPT, only the low-thrust modeling capability is needed, since the Echo trajectories were not optimized.

We also used various other programs developed by NASA to validate the results from S5. Marshall Aerospace VEhicle Representation In C (MAVERIC) is an in-house tool developed at the Marshall Space Flight Center (MSFC) that was nominated for NASA's software of the year award. It is capable of modeling Earth orbits with high-fidelity gravity simulations and has a solar radiation pressure model identical to S5. Princeton Satellite Systems (PSS) also produced the Solar Sail Control Toolbox (SSCT) as part of the In-Space Propulsion solar sail technology effort. SSCT is based on PSS's highly successful Spacecraft Control Toolbox. Finally, we also used some basic formulations of the LaGrange planetary equations as described below for quick, semi-analytical comparisons.

ANALYSIS

Solar Radiation Pressure Model

The solar pressure of the sun at 1 AU is approximately 1358 watts/meter^2. Dividing by the speed of light converts this to 4.56 x 10^{-6} Newtons/meter^2. Designating this value as P and following McInnes[5], the solar radiation pressure force on a sail or any reflecting body can be modeled as:

$$F_n = PA\left((1+rs)\cos^2\alpha) + B_f(1-s)r\cos\alpha + (1-r)\frac{\varepsilon_f\beta_f - \varepsilon_b\beta_b}{\varepsilon_f + \varepsilon_b}\cos\alpha \right)\bar{n}$$
$$F_t = \left(PA(1-rs)\cos\alpha\sin\alpha\right)\bar{t} \qquad (1),$$

where A is area of the sail, r is reflectivity, s is specularity, B_f is the front surface non-Lambertian coefficient (a measure of ideal diffuse reflectivity), B_b is the back surface non-Lambertian coefficient, ε_f is the front surface emissivity, ε_f is the back-surface emissivity, and α is the angle between the sail normal and the sun in the body frame. Finally, $\bar{n}$ and $\bar{t}$ are unit vectors of the normal and tangent to the sail surface, thus f_n and f_t indicate the forces in the direction of these vectors (see Figure 3).

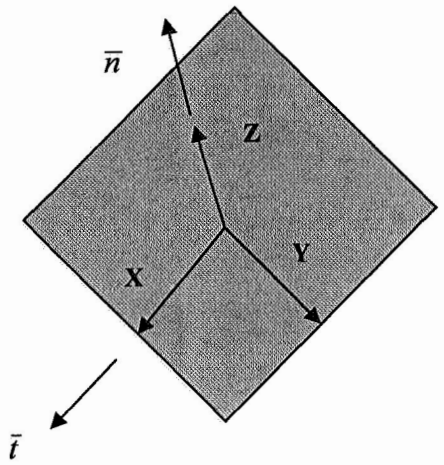

Figure 3 Sail Body Coordinates

Specular reflection is defined as reflection in a single direction that is a function of the incident angle of the light, while light reflecting in a variety of directions is diffuse reflection. For convenience, we point out that the first term in the expression for the normal force in Equation (1) represents the specular reflection, the second term accounts for the diffuse reflection, and the final term accounts for the propulsive effect of thermal re-radiation of heat energy from the backside of the sail (typically a thrust loss). Ideal coefficients for a perfect reflector are presented in Table 1, while Table 2 gives the standard coefficients used by NASA for aluminized Mylar (the material of current sail designs and the Echo balloons).

Table 1 Ideal Reflector Optical Properties

Parameter	Value
r	1.0
ε_b	0.0
ε_f	0.0
β_b	2/3
β_f	2/3
s	1.0

Table 2 Aluminized Mylar Optical Properties

Parameter	Value
r	0.88
ε_b	0.55
ε_f	0.05
β_b	0.55
β_f	0.79
s	0.94

By inspection of Equation 1, we can see that all the non-specular terms cancel out for the ideal sail. Since the coefficients in Table 1 and Table 2 are fairly close to each other, we can conclude that specular reflection will be the dominant term in Equation 1 for aluminized Mylar.

Solar Radiation Pressure on a Sphere

One other aspect of the sail model must be addressed, and that is the shape of the sail. Equation (1) was derived by McInnes for a flat plate. In the case of a more complex sail shape, Equation (1) can be integrated for a series of differential flat plates that approximate the actual shape of the sail, or an analytical expression can be derived and combined with Equation (1), if possible. The Echo balloons are readily modeled as spheres, in fact, early in their respective missions they were close to perfect spheres.

Due to the symmetry of a sphere, two important simplifications can be made immediately. First, the direction the sphere is pointed with respect to the Sun will not matter (unlike a flat plate, for which the direction and magnitude of solar thrust are a function of attitude). This greatly simplifies the computation, since it means that the attitude of the sphere does not have to be modeled by the simulation. Second, all the tangential accelerations on the sphere will cancel out. This means that the tangential component of Equation (1) can be effectively ignored.

Furthermore, the properties in Table 2 for aluminized Mylar include back and front properties because the backside of a solar sail is typically coated with some dark material for thermal reasons, and so possesses different optical and thermal properties. Since all sides of the Echo balloons were coated with aluminized Mylar, we can assume that the frontside and backside emmisivities and the frontside and backside non-Lambertian coefficients are the same. Actually the emissivities were probably slightly different, since emissivity varies as a function of temperature. However, the slight variation in emissivity between the lit and dark sides of the Echo balloons was very likely far less than the variation for typical solar sails for the properties in Table 2, and the thermal component of thrust for a solar sail is typically on the order of 1-2% of total thrust. Thus, we can reasonably ignore the thermal component of the thrust in Equation 1.

We must still assess the effect of the shape of the balloons on the thrust. Since the thermal thrust is neglected, that part of Equation (1) can be eliminated. Furthermore, since the thrust for a sphere is always in the normal direction and along the solar vector in the body frame, we can eliminate the tangential component, and Equation (1) simplifies to:

$$F_n = PA\left((1+rs)\cos^2\alpha + B_f(1-s)r\cos\alpha\right)\bar{n} \qquad (2).$$

Next, we set up the surface integral of the sphere. For a given sphere, a convenient unit vector from the center of the sphere to any point on the surface is:

$$\bar{n} = \sin\phi\cos\theta\ \ \bar{i} \quad \sin\phi\sin\theta\ \ \bar{j} \quad \cos\phi\ \ \bar{k} \qquad (3),$$

where ϕ, θ, and the unit vector $\bar{n}$ are as defined in Figure 4.

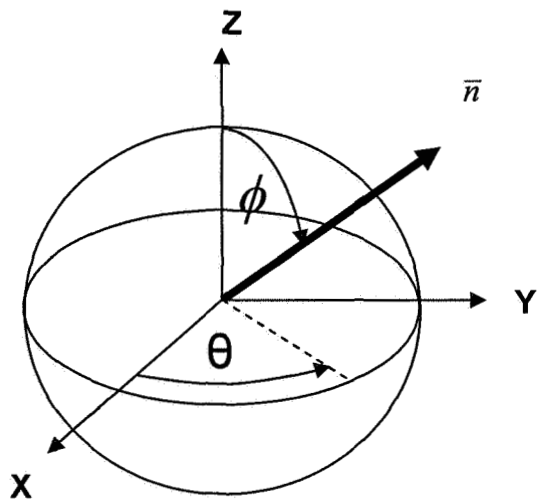

Figure 4 Spherical Body Coordinate System

The equation for a differential area of the sphere in Figure 4 is:

$$dA = R^2 \sin\phi \, d\phi \, d\theta \qquad (4),$$

where R is the radius of the sphere, and dA is the differential area. From McInnes, the definition of the angle α in Equation (1) can be expressed as:

$$\cos\alpha = \bar{s} \bullet \bar{n} \qquad (5),$$

where $\bar{s}$ is the solar vector and $\bar{n}$ is the normal vector from Equation (1) (so α is the incident angle of the sun relative to the normal surface of a flat plate). Now, with Equations (2)-(5) in hand, we can integrate over the surface of a sphere with Equation (2) modeling the optics to obtain an expression for the force generated on a sphere by solar radiation pressure. First, however, we must assume a direction for the solar radiation pressure on the sphere. Since the sphere is fortunately symmetric, the direction of the radiation can be arbitrary. Here, we assume the solar radiation pressure is in the $\bar{i}$ direction. Thus, from Equation (5), the dot product of $\bar{i}$ and Equation (3) yields:

$$\cos\alpha = \sin\phi\cos\theta \qquad (6).$$

Finally, Equations (2), (3), (4) and (6) can be combined into the following:

$$d\bar{F} = PR^2(1+rs)\int_{-\pi/2}^{\pi/2}\int_{0}^{\pi}\left(\sin^4\phi\cos^3\theta \;\; \bar{i} + \sin^4\phi\cos^2\theta\sin\theta \;\; \bar{j} + \sin^3\phi\cos\phi\cos^2\theta \;\; \bar{k}\right)d\phi d\theta$$

$$+ \qquad (7).$$

$$PR^2(1-s)rB_f\int_{-\pi/2}^{\pi/2}\int_{0}^{\pi}\left(\sin^3\phi\cos^2\theta \;\; \bar{i} + \sin^3\phi\cos\theta\sin\theta \;\; \bar{j} + \sin^2\phi\cos\phi\cos\theta \;\; \bar{k}\right)d\phi d\theta$$

All the variables in Equation (7) have been previously defined, however, we note that the limits of integration for ϕ and θ are for only the lit half of the sphere, and the values are consistent with the definition of those angles in Figure (4) and Equation (3). Also, the $\bar{j}$ and $\bar{k}$ components of Equation (7) can be ignored, since by symmetry all the thrust on the sphere should be directly along the solar vector ($\bar{i}$ in this case). However, we performed the rigorous integration for all three directions as a way to check the formulation, and indeed the $\bar{j}$ and $\bar{k}$ components did drop out. We also further tested the validity of Equation (7) by integrating the tangential portion of Equation (1), and again, the tangential force was zero. Finally, we also did a rigorous integration of all axes in the normal direction for an assumed solar vector in the $\bar{j}$ direction as a final check, and the result agreed with our integration for a solar vector assumed in the $\bar{i}$ direction. The result is:

$$\bar{F} = \left[\frac{PR^2\pi}{2}(1+rs) + \frac{2PR^2\pi}{3}(1-s)rB_f \right] \bar{i} \qquad (8).$$

Equation (8) is a useful result, however we can make some further simplifications by assuming that the non-Lambertian coefficient has an ideal value of 2/3, substituting $\bar{s}$ for $\bar{i}$, and rearranging:

$$\bar{F} = PR^2\pi \left[\frac{1}{2} + \frac{4}{9}r + \frac{1}{18}rs \right] \bar{s} \qquad (9).$$

Equation (9) now allows the calculation of an equivalent flat plate area for a sphere. This derivation is necessary because the equations in all the simulations model solar radiation pressure for a flat plate. An equivalent area that will yield the same thrust as the sphere for a flat plate pointed directly at the sun is desired. So, taking Equation (2) with $\alpha = 0$ and $B_f = 2/3$, dividing Equation (9) by Equation(2), setting the ratio of Equation(9) to Equation(2) equal to 1, solving for the equivalent flat plate area and simplifying gives:

$$A_{eff} = \frac{R^2\pi\left(\frac{1}{2} + \frac{4}{9}r + \frac{rs}{18}\right)}{\left(1 + \frac{rs}{3} + \frac{2}{3}r\right)} \qquad (10),$$

where A_{eff} is the flat plate equivalent to use in order to get the proper amount of thrust for a sphere of a given radius and optical properties. For an ideal reflector ($s = r = 1$), the effective flat plate area is $\pi R^2/2$. Using the real optical properties, we find that the diffuse reflection contributes approximately 5% to the thrust of a sphere. We had considered ignoring the diffuse reflection and using an effective area based on only the spectral reflectivity, but Equations (9) and (10) indicated that this would lead to an unacceptably high level of error. Using the real non-Lambertian coefficient from Table 2 only contributed about 0.4% to the overall thrust, so we concluded that we could safely ignore it and assume the ideal value (which simplified Equation (9)).

An interesting result from Equation (9) is that diffuse reflection contributes more to the thrust of a sphere as a percentage of thrust than it does for a flat plate. The curved surface of the sphere means that diffuse radiation from the parts of the sphere that are closer to the unlit side will in fact be reflected in the direction of the sun, thus contributing a positive net thrust that does not exist for a flat plate. For this reason, we need to re-calculate an equivalent flat plate area for the Echo balloons for different optical properties.

Lagrange Planetary Equation Analysis

LaGrange's planetary equations can be used to model perturbation forces to reasonable first-order accuracy for short periods of time. Cooley discusses the use of these equations for solar sails[6]. We used the LaGrange equations for insight into the behavior of all orbital elements but focused particularly on the equation for semi-major axis, because the mean semi-major axis is an important gauge of the accuracy of the integration of small perturbations over a long period of time. The Lagrange planetary equation for semi-major axis is:

$$\frac{da}{d\upsilon} = \frac{2L\rho^2}{\mu(1-e^2)^2}\left[Me\sin\upsilon + \frac{NL}{\rho}\right] \qquad (11),$$

where da/dv is the rate of change of the semi-major axis with respect to true anomaly, ρ is the orbital radius, μ is the Earth's gravitational constant, e is orbital eccentricity, M is solar acceleration in the radial direction (away from the Earth), N is solar acceleration in the direction of the cross product of the angular momentum vector and the radial vector (mostly along the velocity vector), and L is the orbital parameter or semi-latus rectum. Equation (12) below shows the orbital parameter as a function of semi-major axis (a) and orbital eccentricity:

$$L = a(1-e^2) \qquad (12).$$

Using Equation (11), we can make several predictions about the effect of the solar radiation pressure on the semi-major axis of an orbiting Echo balloon without running any simulations. First, we can see that the semi-major axis will mostly change as a function of the transverse solar acceleration N (this is the acceleration mostly in the direction of the velocity vector). This makes sense, since the energy of an orbit will change as result of velocity changes. However there is also the term $Me\sin\nu$ that depends on the acceleration in the radial direction but varies as $\sin\upsilon$, meaning that it essentially averages out over one orbit. So we would expect that the transverse acceleration would be the main perturbation affecting the semi-major axis of the Echo balloons. Similar observations of the effect of the solar radiation pressure perturbation on other classical orbital elements were gleaned from the other LaGrange planetary equations, but we present the semi-major axis equation for purposes of illustrating the technique and also because it was by far the most important of the six equations (one for each orbital parameter) to our analysis.

RESULTS

Our results are all based on historic Echo 1 and Echo 2 trajectories in the Two Line Element (TLE) format obtained from a repository at the Goddard Space Flight Center (GSFC). We had to overcome some initial difficulties with the vectors for two reasons. One difficulty was that the early Echo 1 vectors have some apparent errors. Figure 5 is a plot of height of periapsis (H_P) vs. time that is derived directly from the historical vectors. In Figure 5, we can see that in the first 300 days or so, there are many instances of the H_P parameter staying flat or not changing for a considerable (tens of days) amount of time. This simply cannot be correct, and represents an error of some type in the vectors. The error could have been resident in the original vectors, or could be some product of the archival process. In any case, the problem illustrated in Figure 5 led us to not trust the early Echo 1 vectors, so the analysis focused on the historical state vectors 500 days or so into the mission.

There were some similar issues that arose from not knowing the exact gravity model that was used by the early researchers who calculated the historic Echo state vectors from tracking data. TLE vector sets are currently based on the Standard General Perturbations satellite orbit model 4 (SGP4) gravity model. However this model was not standard for TLE sets[8] until 1970. So there were some questions as to how to make sure the vectors were in the proper format (including issues such as what particular flavor of 1950 coordinate system should be converted to J2000, for instance). What makes these questions interesting in this case is that the Echo 1 balloon was used extensively to help refine early gravity[9], drag[10] and solar radiation perturbation[11] models. So, if the models were in the process of being developed, how could we trust the early vectors? Of course, it is reasonable to assume that the TLE vectors have been converted to the modern format, but there is absolutely no documentation to this effect. In

any case, we were able by various means to determine such format problems were relatively minor compared to other sources of uncertainty.

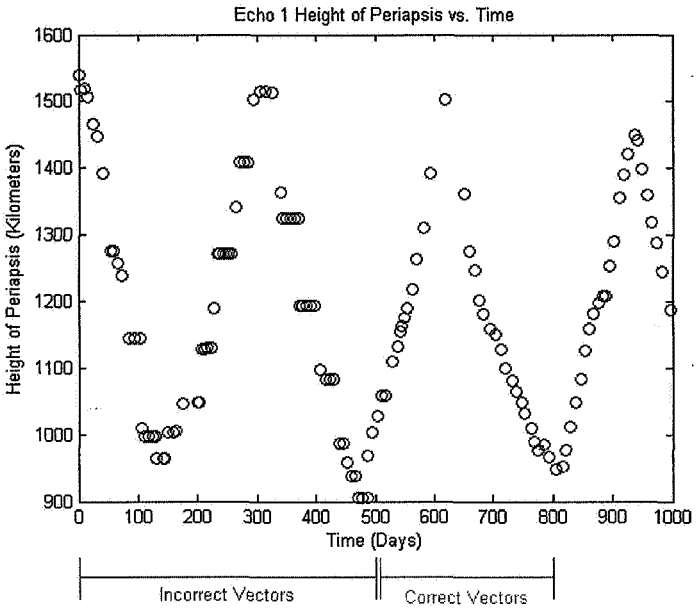

Figure 5: Echo 1 Historical Vector Selection

Some limitations of S5 had to be overcome as well. Specifically, S5 was designed and built to model deep-space missions. The reason that S5 was primarily designed for heliocentric or LaGrange point missions (in short anything but LEO) is because LEO is not an attractive target for solar sail missions due primarily to the rapidly changing solar angle in any Earth orbit other than sun-synchronous, but also due to undesirable environmental characteristics such as atmospheric drag, strong gravity gradient torques, and for certain altitudes, radiation. So no science missions are planned for solar sails in LEO, hence there was no need for an atmospheric drag model (we should note that MAVERIC and SSCT do possess drag models). For this reason, and also because we wanted to focus primarily on the solar radiation pressure effect, the study was limited to altitudes above 1000 km or so. Fortunately, neither Echo 1 nor Echo 2 spent a great deal of the time each was in orbit above this altitude.

S5 also initially did not possess a way of modeling planetary eclipse, for the same reasons it does not have a drag model. However, late in this design study, JPL was able to implement a shadow model on limited funding, for which the authors are grateful. In the meantime, we were able to use an approximate shadow model developed for an earlier version of S5 (the "alpha-test" version) that modeled the planned orbit of the Comsos-1 solar sail of the Planetary Society [ref]. Essentially, the model would lead to shadow entry and exit times being in error by as much as a minute or two, which in turn meant that there was an accumulative error in the solar radiation acceleration over a long period of time. Using Equation (11) in conjunction with output data from S5, we discovered that for Echo 1, the effect of improperly modeling the shadow resulted in overestimates of time of positive energy boosts and underestimates of time of energy decreases, so the net effect was to introduce positive energy growth into the orbit.

We mention the issue with the shadow model because it emphasizes an important point: the primary purpose of this research was to beta-test S5. (A beta-test of software is a test designed to thoroughly "shake it down", testing every requirement and trying to "break it".) So in the case of the shadow model, it was a very positive development to explore the limitations of the approximate shadow model in S5 and discover that by and large it was not acceptable, and JPL was then able implement a more accurate model on what limited budget remained for the development of the software. A second point is that S5 will be used by the ST9 solar sail team if the ST9 mission selects solar sails (currently there are five technology areas competing for the ST9 or Space Technology 9 mission). The Space Technology missions are designed to be flight validations of new technology only, no science required. However, there is a cap on how much can be spent for launching the ST9 mission. Essentially, we are forced to do the flight validation in LEO due to budget constraints. So, given that S5 was not designed for LEO missions, modeling the Echo orbits is a great way to drive out the limitations in S5 that need to be enhanced or corrected prior

to ST9. This will ultimately save time and money if ST9 does select solar sails as the next validation flight, because the limitations of S5 for LEO have now been thoroughly explored.

As mentioned previously, S5 did not include a drag model, although plans are in place to add one for ST9 and this can easily be implemented when ST9 selects solar sails for the next technology validation. So we used Equation (11) in a Matlab script with some calculated density values from historical data to estimate the cutoff altitude above which drag was less than 1% of the solar radiation force. This altitude varied from 1000 km to 1200 km depending on the solar activity. No simulations in this research used vectors below approximately 1100 km.

A final comment on the models in S5 is that it includes various gravity models. Higher-fidelity models were considered, but for many of the longer runs only the J2 model was used to save computation time. (Some earlier scripts also had issues with integration times and step sizes that were not optimal, resulting in long run times). So we should mention that the gravity model was not always of the highest fidelity. However, the J2 model was not a limiting factor in the long-term behavior of semi-major axis, which was the primary parameter of interest, since orbital perturbations from the Earth's gravity field do not affect the secular behavior of the semi-major axis.

In spite of the issues discussed above, the results of modeling the orbits of the Echo 1 and Echo 2 balloons were actually quite good. Figure 6 shows the results of a 223-day simulation of Echo 1 starting around the 520th day of the mission. The plots illustrate that S5, even with the limitations discussed above, was able to model the orbit of the Echo 1 with a reasonable degree of fidelity for over 200 days (the results below are based on the approximate shadow model).

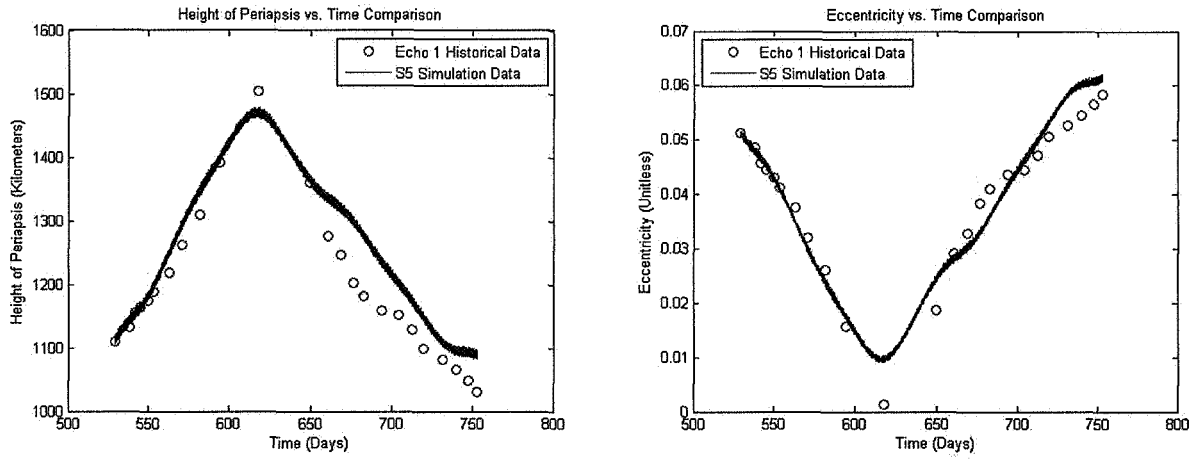

Figure 7 Echo 1 Height of Periapsis and Eccentricity Comparisons

Finally, it should be mentioned that some results from MAVERIC and SSCT and compared favorably with the results from S5.

CONCLUSIONS AND FUTURE WORK

We successfully tested many features of S5, uncovering various problems and reporting them. In some cases fixes were available, and in other cases budget constraints limited the response to documentation for future fixes. The fact that the Echo balloons are historic missions uniquely suited to test solar sail models greatly aided the testing process. The features of S5 that were validated include the solar radiation pressure model, the orbit propagator, various gravity models, and the new shadow model that was incorporated as a result of the Echo modeling. However, we did leave some features untested. For instance, S5 has a complex shape model based on tensors [ref] that was part of the test plan, but due to effort invested in some of the problems discovered, those has not yet been tested. So a future plan is to use the tensor model for shape that is in S5 to model an Echo balloon and compare that result to the effective flat plate model discussed above. We might have tested the shape model earlier in the process, but we wanted to start with more basic aspects of S5 such as the solar radiation pressure model, the gravity model(s) and the basic orbit propagator (all of which were validated). There remains some validation work for even those basic capabilities (for instance, longer-term runs with some of the higher order gravity models).

In terms of modeling the orbits of the Echo balloons themselves, we achieved some useful results but did not get as much insight into the actual behavior of the spacecraft as desired. The ultimate goal of this work would be to do simulations using S5 of a high enough fidelity that would guarantee a good result for the Orbit Determination (OD) portion of ST9. We are probably close with the results in this paper, since the ST9 goal is to determine the thrust of the solar sail to 10%. Along those lines, more could be accomplished as well by comparing S5 to MAVERIC and SSCT. Initially we planned to spend more time with both of those simulations, but issues with S5 and other duties and responsibilities for both authors limited the amount of time available for using those simulations, and we instead had to rely on some Echo runs executed in MAVERIC at a date earlier than most of the S5 work presented in this paper. In the case of SSCT, PSS graciously contributed an Echo simulation as part of their beta-test activity.

Another aspect of the Echo modeling problem that will be pursued at a future date is the Earth albedo model. The Earth reflects as much as 34% of the solar radiation back into space [ref], and this may have had a significant impact on the Echo balloons. We would also like to spend more time investigating some reports that the Echo balloons either lost their shape or that the reflectivity decreased at later dates in the respective missions. Finally, we would also like to incorporate an atmospheric drag model so that we are not limited to only the higher altitudes. For some of these desired simulations, MAVERIC and SSCT will be used as well.

A final conclusion is that the beta-testing of S5 with Echo trajectories provided great input that will save future users of S5, (particularly and potentially in the near future the ST9 team) a great deal of effort. The programmers of S5 now have insight into improvements that will be necessary or highly desired for ST9. Since the purpose of the In-Space Propulsion Solar Sail project, including S5, was to "raise the Technology Readiness Level (TRL) of solar sails to a level of 6" (a level just below a flight validation), the fact that the beta-testing of S5 led to insights for a potential flight project is very appropriate.

ACKNOWLEDGEMENTS

The authors acknowledge the help of Dr. Larry Mullins of MSFC with the shadow model and particularly the derivation of the equations for solar radiation pressure on a sphere. James Evans of JPL and Rob Stough of MSFC also provided valuable assistance with S5.

REFERENCES

[1]G. P Garbe, A. F. Heaton, and J. T. Van Sant, "NASA's Integrated Development of the Solar Sail Propulsion Project", *52nd JANNAF Propulsion Meeting*, Las Vegas, NV, May, 2004.

[2]D. Lichodziejewski, B. Derbes, R. Reinert, K. Belvin, "Bringing an Effective Solar Sail Design Toward TRL 6", AIAA 2003-4659.

[3]D. Murphy, et al, "Progress and Plans for System Demonstration of a Scalable Square Solar Sail", *AAS/AIAA Space Flight Mechanics Conference*, Feb. 2004, AAS 04-105.

[4]J. Ellis, M. Lisano, P. Wolff, J. Evans, J. Bladt, D. Scheeres, L. Rios-Reyes, and D. Lawrence, "A Solar Sail Integrated Simulation Toolkit", *Proc. AAS/AISS Spaceflight Mechanics*, Maui, HI, Feb., 2004, AAS 04-283.

[5]McInnes, C. R., Solar Sailing Technology, Dynamics and Mission Applications, Praxis Publishing, UK, 1999.

[6]Cooley, D. S., "ST9 Mission Design", unpublished.

[7]Thomas, S., Paluszek, M., Wie, B., and Murphy, D., "Design and Simulation of Sailcraft Attitude Control Systems Using the Solar Sail Control Toolbox", AIAA Guidance, Navigation and Control Conference, Providence, Rhode Island, Aug. 16-19, 2004, AIAA 2004-4890.

[8]Hoots, F.R., Roehrich, R. L., "Models for Propagation of NORAD Element Sets", SPACETRACK REPORT NO. 3, Dec. 1980.

[9]Jones, H. M.; Shapiro, I. I.; Zadunaisky, P. E., "Experimental and Theoretical Results on the Orbit of Echo 1", Mar. 20, 1961, SAO SPECIAL REPT.-61.

[10]Romer, M., "Model of the Exosphere in the Altitude Range of 1000-1700 km Calculated from the Change in Orbit of the Echo 1 Satellite", REPT.-997, Jan. 1, 1961.

[11]R. L.; Holdridge, D. B.; Hudson, R. H.; Muhleman, D. O.; Oslund, K. C. "Observed Solar Pressure Perturbations of Echo 1", 13-22 August 1960, NASA-CR-80735.

[12]Prior, E. J., "Earth Albedo Effects on the Orbital Variations of Echo I and PAGEOS I", In-Space Dynamics of Satellites, Proceedings of the Symposium, Prague, Czechoslovakia, May 20-24, 1969.